CHEMISTRY OF MATERIALS

ARTICLE

pubs.acs.org/cm

Synthesis of Stannyl-Substituted Zn_4O_4 Cubanes as Single-Source Precursors for Amorphous Tin-Doped ZnO and Zn_2SnO_4 Nanocrystals and Their Potential for Thin Film Field Effect Transistor Applications

Marianna Tsaroucha, Yilmaz Aksu, Elisabeth Irran, and Matthias Driess*

Technische Universität Berlin, Institute of Chemistry: Metalorganics and Inorganic Materials, Sekr. C2, Strasse des 17. Juni 135, D-10623 Berlin, Germany

Supporting Information

ABSTRACT: The first heterobimetallic alkyl(trimethylstannoxy)-zinc clusters with the formula $[Me_3SnOZnR]_4$ (R = Me **1**, Et **2**) are facile accessible by the Brønsted acid−base reaction of trimethyltin hydroxide with the respective zinc dialkyls ZnR_2 (R = Me, Et). The resulting products **1** and **2** can be isolated as white solids in high yields (>95%) and were characterized by multinuclear NMR, elemental analysis, FTIR spectroscopy, mass spectrometry, and single-crystal X-ray diffraction analyses. They proved to serve as unprecedented low-temperature single source precursors (SSPs) for the fabrication of tin-containing ZnO as well as zinc stannate semiconducting materials and could be successfully utilized in field effect transistor (FET) applications. The thermal degradation of **1** and **2** under dry synthetic air, monitored by thermogravimetric analysis (TGA and TGA-IR), indicates high volatility of the trimethylstannyl group, which turned out to be the key parameter to control the tin concentration in the final semiconducting product. Low temperatures of degradation as well as low heating rates reduce the rate of tin loss and lead to mainly amorphous, nanosized tin-containing zinc oxide materials. Moreover, degradation at higher temperatures (>350 °C) and higher heating rates produces a homogeneous mixture of zinc stannate Zn_2SnO_4 and ZnO as major products. Remarkably, calcination of the latter mixtures at 600 °C favors crystallization and increases the surface area up to 298 $m^2\ g^{-1}$. This unexpected increase in surface area is accompanied by a decrease in the tin concentration owing to the liberation of SnO_2. All of these products were analyzed by multiple techniques including powder X-ray diffraction analysis (PXRD), transmission electron microscopy (TEM), and energy dispersive X-ray (EDX) spectroscopy. Finally, semiconducting thin films of tin-doped ZnO with 1.5 wt % tin were produced, without the use of any additive, through spin-coating of a mixture of precursor **1** and homometallic $[MeZnO^tBu]_4$ and subsequent degradation at 350 °C in dry air. These films can serve as suitable semiconducting layers in FET applications and show a high performance, that is, high electron mobility and homogeneity after annealing at 350 °C in air.

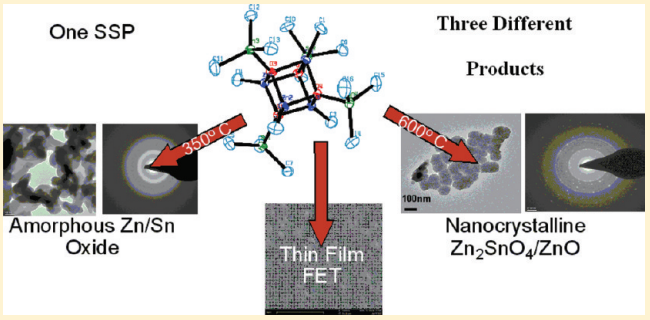

KEYWORDS: transparent conducting oxide, heterobimetallic oxides, optoelectronic device, amorphous conducting films, molecular zinc oxide clusters

INTRODUCTION

The formation of metal−oxygen clusters is of great importance for the development of new multicomponent materials. Specifically, the single-source precursor (SSP) approach,[1a−j] which enables the formation of size- and shape-selective, homo- and heterometal oxide particles, has attracted significant attention in recent years and can be regarded as one of the key techniques for the preparation of functional materials with electronic and catalytic applications. Among homometal oxides, zinc oxide is one of the most important materials that has received growing attention because it can cover a wide spectrum of properties and applications.[1k−1o] ZnO is a well-known wide-bandgap semiconductor with a direct bandgap of 3.30 eV at room temperature and a free exciton binding energy of 60 meV.[1m,2] This makes ZnO a promising material for UV-light-emitting diodes (LEDs),[3] lasers,[4] solar cells,[5] field-emission displays,[6] and gas sensors as well as for applications in catalysis.[7,8]

The electrical, optical, and magnetic properties of ZnO can be significantly modified by doping or combining it with a large variety of elements.[9] In fact, recently, many efforts have been devoted to increase the electronic properties without degrading the transparency, and different synthetic strategies were developed in which ternary M−Zn−O (M = In, Al, Ga, Mn, As, and Sn)[10,11] and multicomponent oxides consisting of combinations of binary systems such as $InGaO_3(ZnO)_5$[12] and $SnGaZnO_4$[13] have been synthesized. Moreover, their suitability as semiconducting

Received: January 27, 2011
Revised: March 24, 2011
Published: April 06, 2011

Scheme 1. Utilization of Organometallic Zn_4O_4 and MZn_3O_4 Cubanes As Low-Temperature, Single-Source Precursors for Respective Preparation of Nano-Sized (a) ZnO, (b) M@ZnO (M = Li, Na, K), and (c) Zn_2SiO_4

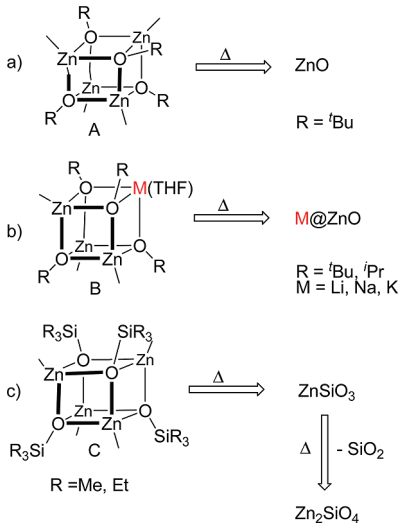

materials in thin film transistors (TFTs) was studied. TFTs based on these materials exhibit more enhanced performances attaining electron mobilities of up to ~108 $cm^2 V^{-1}s^{-1}$, which are superior in comparison to those of conventional Si-based devices. However, the sophisticated processing of these high temperature annealed materials is not suitable for low-cost and large-area depositions. Recently, more efficient methods were employed to fabricate semiconducting systems, exhibiting better compatibility with actual industrial applications. In fact, by spin-coating mixtures of their corresponding precursors, zinc-rich $Zn_7InSn_{10.5}$ and indium-rich $ZnIn_6SnO_{14}$[14a] based TFTs achieving electron mobilities as high as 11.4 $cm^2 V^{-1}s^{-1}$ at relatively low temperatures (~400 °C) were successfully prepared. However, despite their simple preparation and their processing at low temperature, the employment of these indium- and zinc-rich materials, especially for large production of TFT devices is endangered by the scarcity and high price of indium. This situation encourages searching for alternative indium-free ZnO-based low-cost binary semiconducting materials prepared via simple methods and processed at low temperatures.

The Zn/Sn/O ternary system is one of the most promising low-cost candidates of heterometal-containing or doped-ZnO-based semiconducting materials. The great advantage of the use of tin as a second component is its vast abundance, low price, and transparent character as well as its high solubility in the ZnO lattice. This can be attributed to the almost similar ionic radius of Sn^{4+} (0.071 nm) and Zn^{2+} (0.074 nm).[14b] Furthermore, inasmuch as resistance decreases with increased Sn content, this high solubility should allow materials with tunable electronic properties to be synthesized.[15] In fact, this has been demonstrated, by doping ZnO nanowires with Sn, which significantly improved the field emission characteristics.[16] Despite its promising properties, merely a few studies on Sn-containing ZnO materials were reported as yet.[17−19] This may be, in part, due to the lack of reliable straightforward synthetic methods to give pure materials. The classical preparation methods of nanoscaled metal oxides, such as chemical-vapor-synthesis (CVS),[20] flame pyrolysis of precursor solutions,[21] evaporation oxidation of

Scheme 2. Preparation of Heterobimetallic Alkyl-(trimethylstannoxy)zinc Clusters 1 and 2

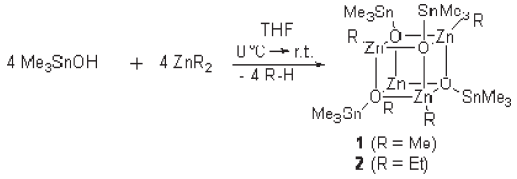

elemental metals, and thermal degradation of inorganic precursors like carbonates, nitrates, and hydroxides,[22] have drawbacks such as expensive and complex equipment, formation of inhomogeneous products with regard to composition and shape distribution, or high processing temperatures.

The SSP approach could be an alternative route to overcome all of these problems[1f−i] and might provide an efficient and facile access to defined Sn-containing ZnO or even to zinc stannate nanoparticles. In this context, we are focusing on the synthesis of well-defined heterobimetallic organozinc alkoxide clusters as versatile molecular SSPs for the preparation of multifunctional, heterobimetallic, or heterometal-doped M@ZnO materials. It has been demonstated that alkylzinc alkoxide clusters $[RZnOR']_4$ with a Zn_4O_4 cubane core **A** can serve as excellent SSPs for the preparation of ZnO nanoparticles (Scheme 1a).[2] Likewise, the substitution of one Zn atom of the Zn_4O_4 cluster core by other metals leads to organobimetallic precursors MZn_3O_4 (**M** = Li, Na, K) **B** (Scheme 1b) for heterometal-containing ZnO-based materials.[9] Moreover, the addition of other desired elements (e.g., Si) in the terminal element-organic groups, such as **C** (Scheme 1c),[23] enables precursors for nanoscaled zinc metallates (e.g., zinc silicates).[20] However, to the best of our knowledge, molecular SSPs for tin-containing ZnO are currently unknown.

Herein, we report the synthesis, characterization, and thermal degradation of the first tin analogues of **C**, that is, compounds **1** and **2** with the formula $[Me_3SnOZnR]_4$ (R = Me **1**, Et **2**), which can be utilized as unexpectedly versatile organometallic, low-temperature degradable precursors for tin-containing ZnO and zinc stannate, including FET applications.

RESULTS AND DISCUSSION

The syntheses of siloxy-substituted Zn_4O_4 cubanes of type **C** have been reported previously, and these precursors have been proven to serve as SSPs in the formation of Zn_2SiO_4 and related materials.[20a,23] The similarities between silicon and tin led us to use a similar methodology to synthesize the tin-containing Zn_4O_4 cubanes **1** and **2** and to study their degradation products. Thus, a solution of trimethyltin hydroxide in tetrahydrofuran (THF) was added dropwise to a solution of the appropriate ZnR_2 precursor (R = Me or Et) in THF at 0 °C (Scheme 2).[23] The reaction mixtures were stirred and allowed to warm to room temperature overnight. After removal of all volatile components in vacuo, the crude products were dissolved in toluene and stored at −20 °C to give the corresponding products **1** and **2** as colorless crystals in very good yields (93−95%). Compounds **1** and **2** are sensitive toward air and moisture but stable in solution or in the solid state under an inert atmosphere.

The ^1H, ^{13}C, and ^{119}Sn NMR spectra of both compounds show similar features and are consistent with their proposed structures. The respective NMR spectra of **1** and **2** are shown in

dx.doi.org/10.1021/cm200282w |Chem. Mater. 2011, 23, 2428–2438

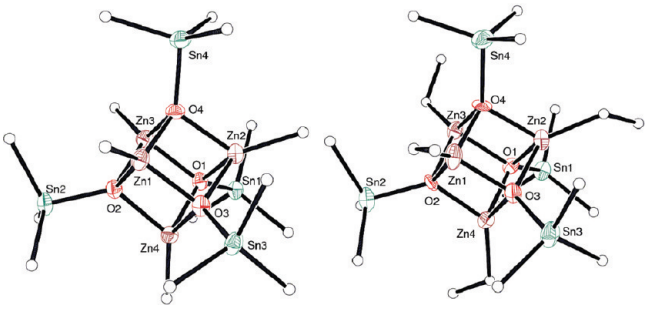

Figure 1. Molecular structures of compounds **1** (left) and **2** (right). Thermal ellipsoids (except C atoms) are drawn at the 50% probability level. Hydrogen atoms and toluene solvent in the crystal are omitted for clarity.

Table 1. Selected Bond Lengths [Å] and Angles [°] for 1 and 2

	1	2
Zn(1)−O(2)	2.042(3)	2.072(10)
Zn(1)−O(3)	2.045(3)	2.037(11)
Sn(1)−O(1)	1.997(3)	1.999(9)
Sn(2)−O(2)	2.001(3)	2.017(9)
Sn(3)−O(3)	2.006(3)	2.003(9)
Sn(4)−O(4)	2.001(3)	1.996(9)
O(4)−Zn(1)−O(3)	86.24(13)	85.9 (4)
Zn(1)−O(2)−Zn(3)	86.85(15)	86.0(15)
Sn(1)−O(1)−Zn(4)	124.52(18)	123.0(5)
Sn(2)−O(2)−Zn(3)	120.76(15)	129.4(5)
Sn(3)−O(3)−Zn(4)	127.39(17)	122.5(5)
Sn(4)−O(4)−Zn(1)	123.52(18)	122.5(5)

Supporting Information S1 and S4, respectively. In the ^{1}H NMR spectrum of compound **1** (Supporting Information S1), two singlets appear at δ = 0.36 and −0.42 ppm, respectively, with an integration ratio of 3:1. The larger signal at δ = 0.36 ppm shows characteristic $^{117/119}$Sn-satellites with coupling constants of $|^{2}J$ (^{1}H $^{117/119}$Sn)| = 27.58 Hz/28.80 Hz, which are similar to values reported for related stannoxy compounds.[24] The high-field resonance at δ = −0.42 ppm is typical for protons of the Zn-methyl moiety.[25] The ^{1}H NMR spectrum proves that **1** is highly symmetrical and contains a 1:1 ratio of zinc and tin as expected for the desired cubane. The ^{13}C NMR spectrum has similar features, showing a signal at δ = −2.44 ppm, corresponding to the $SnCH_3$ groups $|^{1}J(^{13}C\ ^{117/119}Sn)|$ = 186.18 and 194.86 Hz, and another signal at δ = −14.01 ppm, which is typical for a methylzinc moiety (Supporting Information S1). Likewise, there appears one singlet resonance in the ^{119}Sn NMR spectrum (Supporting Information S1), which is shifted downfield (δ = 139.29 ppm) in comparison with the starting material Me_3SnOH (δ = 105.5 ppm).[26]

The tetrameric aggregation of the $MeZnOSnMe_3$ units in **1** and **2** were confirmed by mass spectrometry. Thus, EI-MS (electron impact mass spectrometry) measurements of **1** and **2** revealed ion peaks at m/z 1027 and 1079, respectively, which correspond to the attributed tetrameric compounds with the loss of a single R group at zinc (R = Me for **1** and R = Et for **2**, respectively). Additionally, using the milder chemical ionization CI-MS technique, the expected molecular ion peaks at m/z = 1045 for **1** (Supporting Information S2) and 1096 for **2** were detected (see Supporting Information S2 and S6).

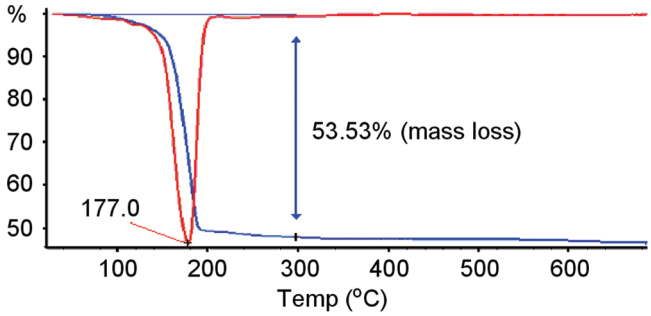

Figure 2. TGA and DTG curves obtained from the degradation of **1** in dry synthetic air.

The structures of **1** and **2** were unambiguously determined by single-crystal X-ray diffraction analysis (Figure 1). Crystals of **1** and **2** were obtained by cooling saturated solutions in toluene to −20 °C (see Supporting Information Table S1−2). Both compounds crystallize in the monoclinic space group $P2_1$. In the distorted Zn_4O_4 cluster core, the Zn−O−Zn angles are smaller than 90°(86−87°) and the Zn−O distances are between 2.04 and 2.07 Å (see Table 1), which is typical for endocyclic Zn−O bonds.[25−30] The Zn−O bond lengths in **1** and **2** are also slightly shorter than those of substituted Zn_4O_4 cubanes **C**, i.e., 2.07−2.10 Å for $[Et_3SiOZnMe]_4$.[23,28] The Sn−O bond distances in **1** and **2** (2.05−2.07 Å) are slightly shorter than in related trimethyltin alkoxides (∼2.2 Å).[29] To find out whether the tetrameric structure is retained in hydrocarbon solutions, the $^{13}C\{^{1}H\}$ solid state magic angle spinning (MAS) NMR spectrum of **1** was measured and compared to the spectrum obtained in C_6D_6 solutions (see Supporting Information S3). The lack of significant differences in these two spectra indicates strongly that the $[Me_3SnOZnMe]_4$ cubane structure does not dissociate in aromatic solvents, which is supported by cryoscopic measurements confirming the tetrameric cubane structure.[30]

THERMAL DEGRADATION OF 1 AND 2

In order to learn whether the new compounds **1** and **2** are suitable SSPs for the preparation of Sn-containing ZnO and/or zinc stannates, their thermal degradations were examined by thermogravimetric analysis (TGA)-differential thermogravimetry (DTG) studies. The precursors were heated using standard conditions (5 K/min from 25 to 600 °C) under dry synthetic air (20% O_2, 80% N_2), which lead to yellow powders. The TGA-DTG curve for **1** is shown in Figure 2. The degradation maximum occurs at 177 °C and corresponds to the elimination of the organic residues. Interestingly, this is at a significantly lower temperature than the maximum weight loss temperature for pure organosubstituted Zn_4O_4 cubanes (242−263 °C).[31] For precursor **2**, the degradation maximum is observed at 107 °C (see Supporting Information S9).

The low processing temperatures of **1** and **2** could be a great advantage for the formation of semiconducting metal oxide thin films on organic polymers for optoelectronic devices. Remarkably and in contrast to the degradation of organosilyl substituted Zn_4O_4 cubanes **C**,[20] there is a large difference between the calculated (75.31%) and the experimental remaining mass (46.47%) for

dx.doi.org/10.1021/cm200282w |Chem. Mater. 2011, 23, 2428–2438

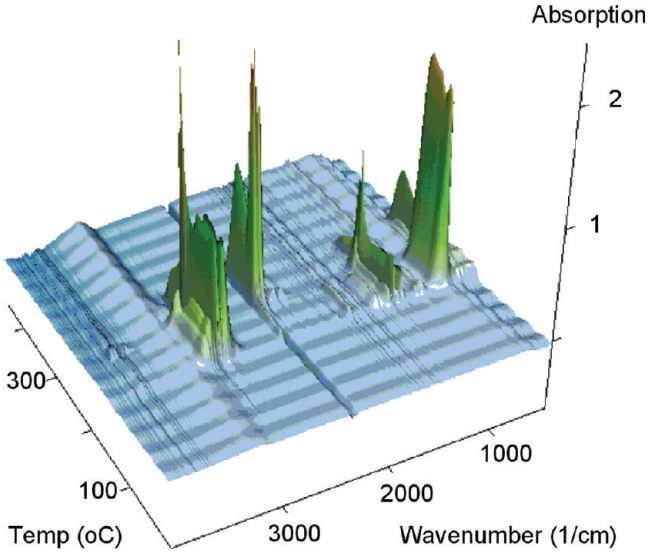

Figure 3. TGA-IR measurements taken during the degradation of **1** in dry synthetic air.

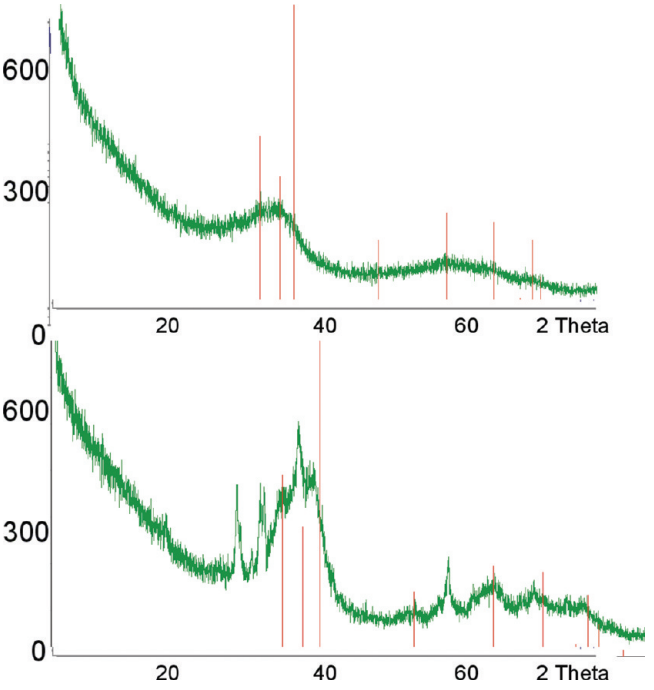

Figure 4. PXRD patterns of the tin-containing zinc oxides obtained from the thermal degradation of **1** in dry synthetic air at (top) rt→ 150 °C (2 h), heating rate 5 K/min; (down) rt → 350 °C (2 h) with a heating rate of 5 K/min [ICDD PDF for ZnO 75−1526 (red)].

1 (similar results were obtained for **2**; see Supporting Information S6). This indicates that not only the organic groups are lost during the thermal degradation but also some Sn-containing volatiles. This was confirmed by TGA-IR measurements, which clearly shows the loss of Me_3SnOH (characteristic wavenumbers are 3015 (CH_{str}), 2917-(CH_{str}), 1305(SnO_{str}), 770 (CH_{bend}), and 529 (CSn_{bend}), cm^{-1}) beginning at 155 °C. At 170 °C methane and between 215 and 255 °C, continuously, CO_2 (2640 (CO_{str}), 546 cm^{-1} (CO_{bend})) and methane (3000 (CH_{str}), 1300 cm^{-1} (CH_{str})) were detected

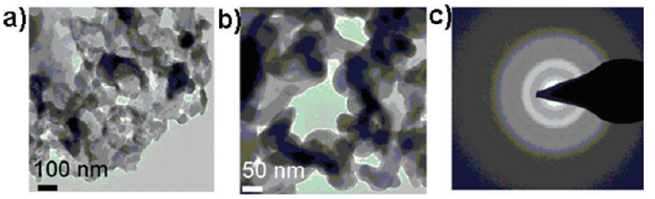

Figure 5. TEM images (a, b) and diffraction pattern (c) of the tin containing zinc oxide material obtained from the thermal degradation of **1** in dry synthetic air at rt → 150 °C (2 h) with a heating rate of 5 K/min.

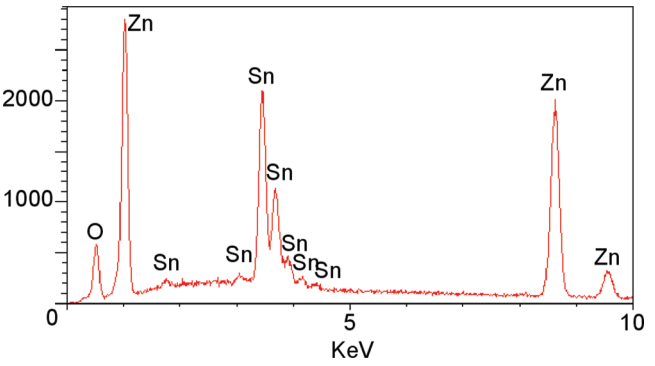

Figure 6. EDX spectrum of the tin containing zinc oxide material obtained from the thermal degradation of **1** in dry synthetic air at rt → 150 °C (2 h) with a heating rate of 5 K/min.

(Figure 3). For full details on the degradation of **1** and **2**, see the Supporting Information S7.

■ MATERIALS DERIVED AT DIFFERENT TEMPERATURES T_{MAX}

Since the TGA-IR results indicated more tin is eliminated at higher decomposition temperatures, it seemed likely that the tin concentration of the resulting products could be regulated using different decomposition temperatures (T_{max}). Therefore, the degradation of **1** was performed at T_{max} = 150 and 350 °C, respectively, which led to pale yellow powders. The powder X-ray diffraction analysis (PXRD) pattern of **1** decomposed at T_{max} = 150 °C exhibits very broad reflexions, which indicates a high content of amorphous material (Figure 4). This is confirmed by transmission electron microscopy (TEM) measurements (Figure 5). The respective TEM images clearly show aggregated amorphous particles with virtually no grain boundaries. The material was further analyzed by EDX (energy dispersive X-ray) spectroscopy and ICP-OES (inductively coupled plasma-optical emission spectroscopy). As expected, the EDX spectrum confirmed the presence of both tin and zinc (Figure 6; see also Supporting Information S9−11). Furthermore, the ICP-OES measurements revealed that the Sn concentration is 65 wt %, which is quite high compared to samples treated at higher temperatures (Table 2). In contrast, the material formed by heating **1** to T_{max} = 350 °C is more crystalline, as indicated by PXRD analysis (see Figure 4 (down)) but is contaminated with carbon impurities. The ICP-OES analysis of the latter material revealed that the Sn-concentration decreases to only 52 wt %.

As mentioned above, the TGA measurements indicated that not only the organic groups but also a significant amount of tin is lost through elimination of Me_3SnOH. In order to learn whether

dx.doi.org/10.1021/cm200282w |*Chem. Mater.* 2011, 23, 2428–2438

Table 2. Surface Area and Tin Content of Materials Obtained by Degradation of 1 in Dry Synthetic Air rt → 600°C with Various Heating Rates and Times

heating rate (K/min)	heating time (h)	0	2	4	6	12	24	36
5	surface area[a]	22.342	29.090	30.346	37.547	135.143	184.401	194.311
	wt % Sn[b]	46.5	31.81	30.98	30.07	24.51	22.42	10.14
15	surface area[a]		70.571	71.473	107.06	194.401	202.354	252.026
	wt % Sn[b]		27.21	25.83	25.12	20.05	12.23	7.18
30	surface area[a]		128.915	134.852	151.157	192.321	228.747	298.783
	wt % Sn[b]		25.01	22.71	20.14	12.45	9.31	4.82

[a] BET-surface area (m^2/g). [b] wt % Sn measured by ICP-OES.

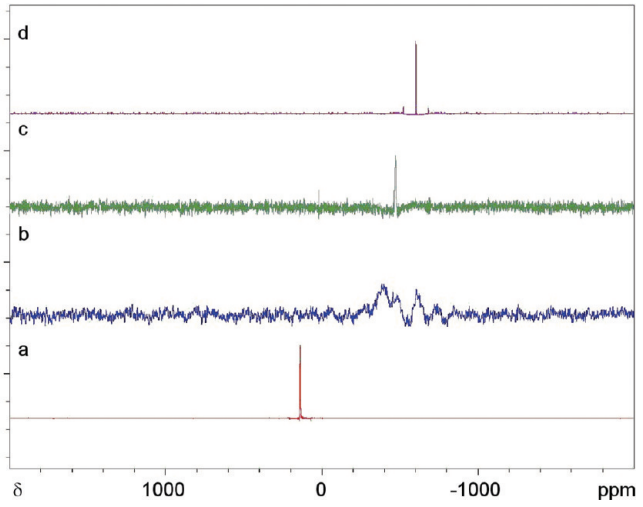

Figure 7. (a) $^{119}Sn\{^1H\}$ MAS NMR spectrum of **1**, (b) $^{119}Sn\{^1H\}$ MAS NMR spectrum of the material resulting from degradation of **1** in dry synthetic air at T_{max} = 150 °C, (c) T_{max} = 600 °C, and (d) at T_{max} = 600 °C for 36 h (heating rate always 5 K/min).

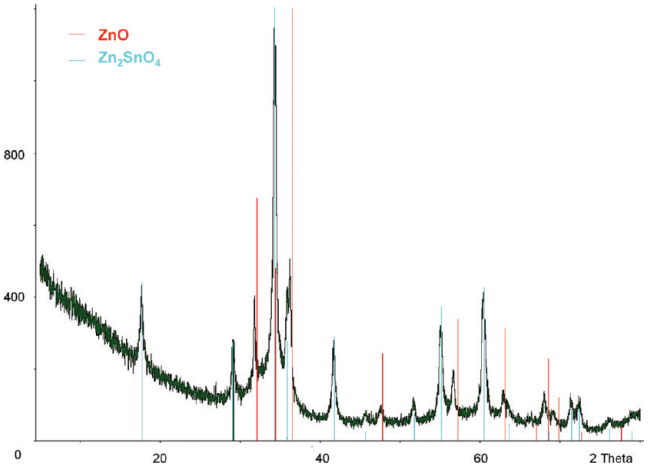

Figure 8. PXRD pattern of 1 decomposed in dry synthetic air; rt → 600 °C (2 h); heating rate, 5 K/min. The peaks for ZnO and Zn_2SnO_4 are shown in red and blue, respectively, red [ICDD PDF for ZnO 75-1526 and for Zn2SnO4 74-2184], the peak at 2 theta = 28 corresponds to the Si support.

the materials from the degradation of **1** still contain organic impurities, IR spectra of all the materials were recorded. The spectra for all of the materials are very similar and show two main features: They contain Sn−O and Zn−O stretching modes which appear at ν = 1570−1410 cm^{-1} and 3216−3640 cm^{-1}. Additionally, signals with relatively low intensity at ν = 2850 and 3490 cm^{-1} were observed which can be assigned to C−H and O−H stretching modes of remaining traces of impurities. Elemental analysis confirmed that the percentage of carbon in all the samples is less than 0.3%, which indicates that nearly all the organic groups from the SSPs were successfully removed during thermal treatment (for IR and elemental analysis data, see the Supporting Information S12).

^{119}Sn MAS NMR has been proven to be exceptionally sensitive to changes in the local structure around tin atoms.[32] Figure 7 compares the ^{119}Sn MAS NMR spectra of **1** before degradation and the different final materials derived at various degradation temperatures and annealing times. For the organometallic precursor, the solid state NMR gives a sharp signal at δ = 137.00 ppm (Figure 7a), which is characteristic for the tetrameric compound and very similar to the solution ^{119}Sn NMR spectrum as shown in Supporting Information S3. The degradation of the precursors at temperatures below 350 °C leads to amorphous Sn-containing ZnO products as indicated by PXRD measurements (Figure 4), which exhibit only reflexes belonging to ZnO. The presence of tin in the final materials was confirmed by ICP-OES measurements. The ^{119}Sn MAS NMR spectrum of the samples annealed at 150 °C show a signal at −386.04 ppm which is shifted to a resonance at δ = −388.2 ppm by increasing the annealing temperature to 350 °C, as illustrated in Figure 7b.

At annealing temperatures above 350 °C, the formation of Zn_2SnO_4 is observed. PXRD analysis revealed that the material resulting at T_{max} = 600 °C is a mixture of crystalline Zn_2SnO_4 and ZnO. To confirm that no other amorphous tin components are present in the as-prepared samples, a solid state $^{119}Sn\{^1H\}$ MAS NMR spectrum was recorded (Figure 7c). The spectrum shows merely one broadened singlet at δ = −472 ppm, which is very characteristic for stannates[33] especially Zn_2SnO_4[34] (δ = −477.0 ppm) and is significantly downfield shifted from SnO_2 (δ = −604.5 ppm), the only other reasonable tin-containing decomposition product.

Thermal treatments at temperatures of 600 °C or higher for long time (36 h) lead to a phase segregation, and the formation of SnO_2 is observed as confirmed by the ^{119}Sn MAS NMR spectrum, in which a sharp peak at δ = −604.5 ppm very characteristic for SnO_2 is observed (Figure 7d).[33,35−38]

The formation of Zn_2SnO_4 from the degradation of **1** and **2** under the aforementioned conditions is not surprising. As already revealed, the degradation of **C** (see Scheme 1) leads, dependent on the thermal conditions, to $ZnSiO_3$ (at low temperature) and α- or β-Zn_2SiO_4 and amorphous silica (at high temperature). Furthermore, we already reported that the decomposition of

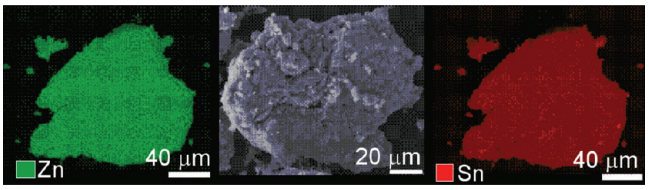

Figure 9. SEM-element-mapping images obtained from the sample prepared by the degradation of **1** in dry synthetic air rt → 600 °C (2 h), heating rate of 5 K/min.

molecular Zn/Mn SSPs leads to analogous materials ($ZnMnO_3$ or Zn_2MnO_4), dependent on the elemental ratios of the SSPs used.[12]

In our case, the continuous loss of tin during the annealing process inhibits the formation of $ZnSnO_3$ due to a stoichiometric deficiency. Crystalline Zn_2SnO_4[35] could be observed only at high temperatures (600 °C; see Figure 8). At temperatures lower than 600 °C, no evidence of crystalline $ZnSnO_3$ or Zn_2SnO_4 could be detected.

The resulting $ZnO-Zn_2SnO_4$ mixtures could be of interest because each component has a wide variety of applications. Both ZnO and Zn_2SnO_4 are transparent semiconducting oxides (TCOs).[40,41] Zn_2SnO_4 is a direct band gap semiconductor (E_g = 3.60 eV) with high electron mobility, high electrical conductivity, and low visible absorption.[39,40] Thus, Zn_2SnO_4 can be employed as the anode in photoelectrochemical cells and Li-batteries, in sensors for combustible gases and gas humidity, and in catalysis.[35−38] TCOs can be used as thin film photovoltaic devices[42] and flat-panel displays, which are highly relevant in manufacturing.[43]

This two-component $ZnO-Zn_2SnO_4$ material may have interesting properties, and varying the decomposition parameters may lead to different ZnO-based materials with adjustable (e.g., optoelectronic) properties all from one precursor. Therefore, the thermolysis of **1** was studied more extensively at different heating rates (5−30 K/min) and annealing times (2−36 h). Variation of the oxygen percentages in the gas stream used for the degradation of **1** and **2** shows no significant influence on the properties (composition, crystallinity, and morphology) of the final materials. Oxygen concentrations under 20% gave materials contaminated with carbon. The degradation under exclusion of oxygen (in a pure nitrogen atmosphere) leads at 600 °C to the same materials (Zn_2SnO_4 and ZnO) but with high carbon impurities (of >10%, measured by elemental analysis). For each of the respective degradation conditions, the BET (Brunauer-Emmet-Teller) surface areas were measured (under nitrogen absorption at 78K), as well as the corresponding Sn concentrations by ICP-OES (Table 2). As one can see, the longer the precursor is heated at 600 °C, the larger the surface area becomes. This increase in surface area is accompanied by a decrease in the Sn concentration. During the heating process, especially at high temperatures and extended heating times, the sublimation of a white compound on the quartz tube is observed. PXRD analysis of this substance revealed the presence of SnO_2, which was also confirmed by XRF measurements. The sublimation of SnO_2 is favored at high temperatures and by the increased partial pressure in the quartz tube (see Supporting Information S13). The highest Zn_2SnO_4 proportion can be found by PXRD and ICP-OES in the sample heated for 6 h, applying a heating rate of 5 K/min.

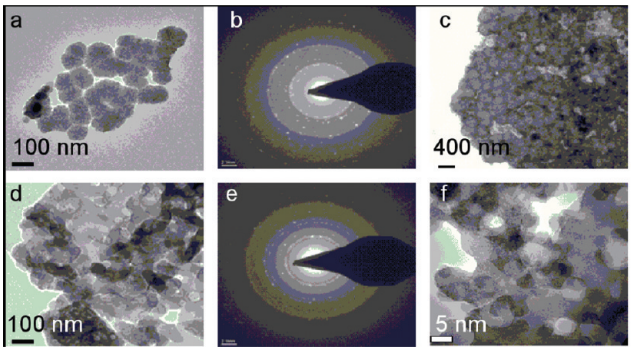

Figure 10. TEM images (a, c, d, f) and diffraction patterns (b, e) of the materials produced by degradation of **1** in dry synthetic air rt → 600 °C (2 h) (a, b, c) and (36 h) (d, e, f) with a heating rate of 5 K/min.

All of the materials were also characterized by SEM (scanning electron microscopy) mapping, which showed the metals to be highly dispersed. Typical SEM images for samples with a heating rate of 5 K/min (rt → 600 °C (2 h)) are shown in Figure 9.

The PXRD diffraction pattern and TEM images revealed that all the materials produced were crystalline with well organized domains. Representative examples can be found in Figures 13 and 14. Interestingly, when comparing the TEM images of the material heated for 2 and 36 h, the difference in porosity, as measured in the BET experiments, is actually visible (Table 2). The increase in porosity can be explained in conjunction with the decreasing tin content. As was seen by TGA-FTIR studies, at the beginning of the degradation (100−300 °C; Figures 2 and 3), the Me_3Sn residue acts as a leaving group and leaves without precipitating on the walls of the tube.

Whereas at higher temperatures and prolonged heating times, tin is continuously lost in the form of SnO_2, which sublimes onto the quartz tube (see the Supporting Information S13). The tin loss is gradual, and the material has time to form. Therefore, the tin moieties act as templates to generate the observed porous structure upon prolonged heating. The heating time has a significant effect on the porosity and tin content of the final material. This is demonstrated clearly: by adjusting the degradation conditions, the properties of the material can be tuned. Therefore, we varied the heating rate (5, 15, and 30 K/min) and once again looked at heating times from 2 to 36 h (Table 2 and Figure 10).

At higher heating rates, the previous trends in porosity and tin content continue, i.e., increased porosity and decreased tin content. At these higher heating rates, the effect is accentuated particularly in relation to the porosity. For example, at 5 K/min after 6 h, the surface area is 37.5 m^2/g while at 15 K/min the surface area is almost triple (107.1 m^2/g) and even higher by heating at 30 K/min (151.2 m^2/g; Table 2). Such high surface area ZnO-based materials are usually achieved by more complex templating techniques; however, here, we were able to obtain high porosity from a SSP, without the use of a template.[44]

While the tin content also decreases with increased heating rate, this effect is not as marked as the change in the surface area. For example, the difference between 5 and 15 K/min (after 6 h) is only 5 wt % (30−25 wt %, as measured by ICP-OES). Having established that the materials synthesized at higher heating rates are highly porous and contain Sn, we set about to identify the crystalline products by PXRD (Figure 11, which only shows ZnO. This indicates that the Sn^{4+} atoms are successfully

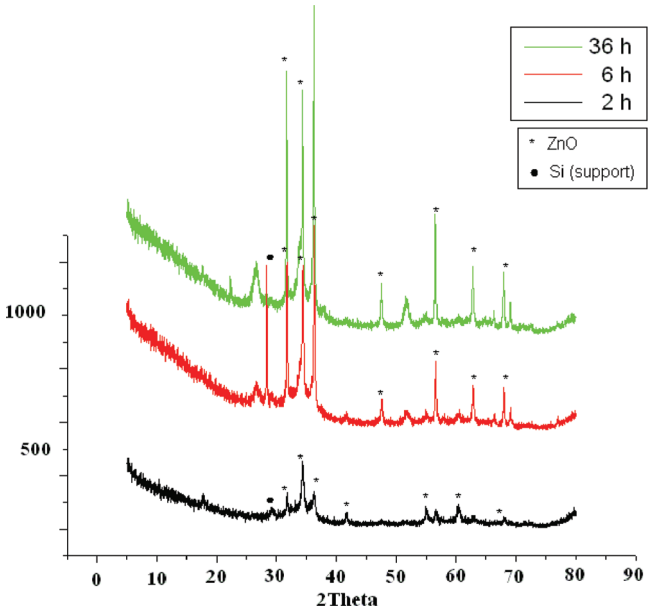

Figure 11. PXRD patterns of the material obtained from thermal degradation of 1 in dry synthetic air; rt → 600° with a heating rate of 30 K/min after 2, 6, and 36 h.

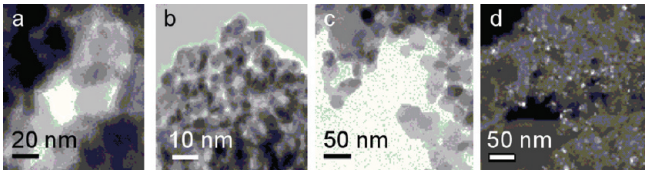

Figure 12. TEM images (a, b, c) and dark field image (showing the crystalline domains, d) of ZnO-based nanopowders from the degradation of **1** in dry synthetic air; rt → 600 °C (36 h) with a heating rate of 30 K/min.

incorporated in the ZnO network or are present as amorphous SnO_2.

The physical characteristics of the nanopowders can be seen by the TEM images (Figure 12). They show small particles (25−30 nm) of highly nanocrystalline material, which are clearly evident in the dark field image (Figure 12d). This indicates that the Sn atoms are very soluble and homogenously dispersed in the ZnO matrixes.

THIN FILM APPLICATIONS

As mentioned above, the as-prepared amorphous ZnO/Zn_2SnO_4 mixtures could be promising materials, particularly for semiconductor applications. To date, the majority of research in this field has focused on ZnO,[32] and indium−zinc oxide (IZO)-based[33] and indium−zinc-tin-based thin film field effect transistor (FET) applications.[10,14] Therefore, we set about to prepare thin films of our new amorphous Sn-containing ZnO materials in order to study its performance for semiconducting applications. However, a tin content of 65 or 52 wt % is too high for a doped material. Additionally, while tin is very cheap, its toxicity makes the use of smaller quantities very desirable for functional materials.

Table 3. Electrical Performance of Thin Film Transistors Fabricated from Precursor 1 Annealed at 350°C

sample	annealing temperature (°C)	μ_{FET} ($cm^2/(V\,s)$)	I_{on} (A)	$I_{on/off}$ (A)
1	350	1.0×10^{-1}	3×10^{-4}	1.0×10^{4}
2	350	1.0×10^{-2}	2×10^{-5}	1.0×10^{3}
3	350	3.5×10^{-2}	2×10^{-5}	1.0×10^{3}

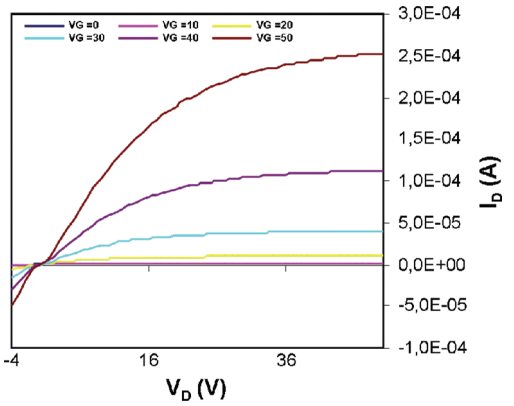

Figure 13. Drain current versus drain to source voltage (I_D-V_D) output characteristics of the TFT as-prepared Sn@ZnO thin films on Si-wafers prepared from **1** and $[^tBuOZnMe]_4$ and annealed at 350 °C in air.

Thin films were prepared by spin coating the precursor **1** in toluene on silicon wafers under controlled conditions, e.g., in nitrogen atmosphere (O_2 < 1 ppm, H_2O < 6 ppm), followed by thermal treatments in air at temperatures ranging from 150 to 650 °C. Investigation of the morphologies and electrical properties of the as-prepared films after annealing in air revealed clearly that the resulting tin containing ZnO-based film with a maximum tin concentration of 5% prepared at annealing temperatures of 350 °C is the more suitable sample for a semiconducting material for TCO applications. In order to decrease the tin concentration in the final products, precursor **1** was diluted with the well-known Zn_4O_4 cubane $[^tBuOZnMe]_4$ by mixing both of them in toluene to give varying Sn/Zn ratios.[2] In this fashion, we were able to prepare thin films with the desired tin concentration.

On the basis of UV−vis spectra, the as-prepared tin-doped ZnO thin films show transmittance over 90% in the visible range (see Supporting Information S14). The resulting films (30−50 nm thickness) with different tin content ranging from 0.5 to 5 wt % were obtained after calcination and exhibited good adhesion on the Si substrates. The FET substrate consists of heavily doped silicon coated with a 240 nm SiO_2 layer, on which gold electrodes were deposited with an intermediate adhesive of indium−tin oxide (ITO). The electronic performance of the as-prepared thin films was studied. The thin film transistors prepared at 350 °C showed the best FET characteristics. Table 3 summarizes the FET characteristics of the as-prepared thin films. The best results (Figure 13) were obtained with the sample with a tin concentration of 1.5 w%.

The best as-deposited thin film exhibits an electron mobility of μ = 0.1 $cm^2/(V\,s)$ with an on−off current ratio of 10^4. Figure 13 shows the drain current as a function of drain voltage

dx.doi.org/10.1021/cm200282w |*Chem. Mater.* 2011, 23, 2428–2438

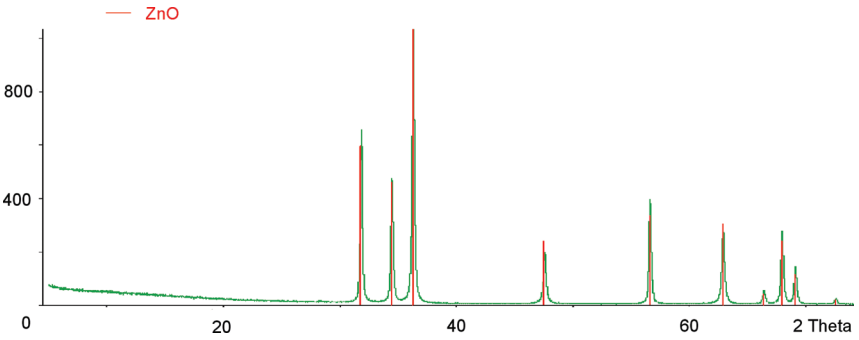

Figure 14. PXRD pattern of Sn-doped ZnO (1.5 w% Sn) recorded from the thin film prepared by the degradation of 1 and $[^tBuOZnMe]_4$ in dry synthetic air at 350 °C). The reflexes for ZnO are shown in red [ICDD PDF for ZnO 75-1526].

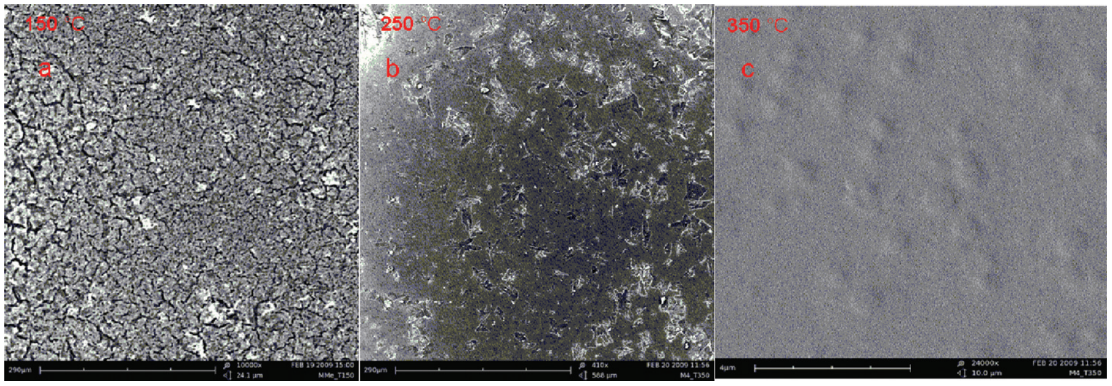

Figure 15. SEM micrographs of the as-prepared Sn-doped ZnO thin films on Si-wafers prepared from **1** and $[^tBuOZnMe]_4$ and annealed at different temperatures in air.

(I_D-V_D characteristics) with varied gate voltage (V_G) for FET devices (Figure 13, see also Supporting Information S15).

There has been one report of an amorphous Sn-doped ZnO FET with better field-effect mobility (μ = 1.1 cm2/(V s)) and an on−off ratio of 10^6. However, these results where obtained with significantly higher tin content (10−40 wt %), and a much higher calcination temperature was required (>500 °C).[34,45]

The chemical composition of the thin films were probed by PXRD. Remarkably, the diffraction pattern shows only signals for ZnO because of the similarity between the ionic radius of Sn^{4+} (0.071 nm) and Zn^{2+} (0.074 nm),[46] which makes it highly likely that the Sn^{4+} centers simply substitute Zn^{2+} sites in the ZnO lattice at this very low tin concentration (1.5 wt %; Figure 14).[34]

SEM images were taken to investigate the physical structure of the thin films, and they show a compact structure with homogeneous morphology and a very smooth surface (Figure 15c). Films prepared at temperatures lower than 350 °C were not homogeneous, probably owing to incomplete formation of the ZnO network (see Figure 15a,b), whereas at higher temperatures cracking was the main problem, preventing good film quality and electrical conductivity.

The low temperature degradation of **1** has proven to be a promising method for facile preparation of amorphous, Sn-doped ZnO thin films with high electron mobility and without grain boundaries. Furthermore, the SSP methodology simplifies[47,48] the preparation of Sn-doped ZnO with variable tin concentrations at significantly lower processing temperature. Similar preparation of thin films based on precursor **2** did not give the electron mobility results obtained from precursor **1**, presumably because of the higher carbon content of **2** and a higher content of impurities in the resulting film.

CONCLUSION

We have successfully reported the high yield syntheses of the first heterobimetallic trimethyltin-substituted alkyl(trimethylstannoxy)zinc single-source precursors (SSPs) **1** and **2** by a one-pot reaction procedure. Thermal degradation of **1** and **2** under different conditions give rise to amorphous Sn-containing ZnO or crystalline mixtures of Zn_2SnO_4 and ZnO, which are highly promising materials for thin film electronic applications. While the thermal treatment of the precursors at low temperatures (≤350 °C) leads to amorphous Sn-containing ZnO, their degradation at high temperatures (600 °C) favors crystallization and leads to a highly dispersed crystalline mixture of Zn_2SnO_4 and ZnO with increasing Zn_2SnO_4 content at longer calcination times. Thus, the SSP method has proved to be a facile route to produce homogeneous mixtures of Zn_2SnO_4 and ZnO. Finally, thin films of Sn-doped ZnO were probed for FET applications. The films can be produced very easily and with varying tin concentrations through deposition of mixtures of **1** and $[MeZnO^tBu]_4$ by spin-coating on *n*-doped Si-wafers and subsequent calcination in dry air at 350 °C. The obtained FET devices show high electron mobilities and on/off ratios due to the high homogeneity of the amorphous material and the lack of grain boundaries.

dx.doi.org/10.1021/cm200282w |*Chem. Mater.* 2011, 23, 2428–2438

EXPERIMENTAL SECTION

General Remarks. All reactions were performed under anaerobic conditions using the Schlenk technique. Solvents were refluxed over an appropriate drying agent (sodium and benzopghenone), distilled, degassed, and N_2 saturated prior to use. Trimethyltin hydroxide is commercially available from Alfa Aesar.

The NMR data (TMS standard) were recorded on Bruker ARX 200 [200 MHz (^{1}H); 50.3 MHz (^{13}C)], AM 400 [400 MHz (^{1}H); 100.64 MHz (^{13}C)], and AV 400 [400 MHz (^{1}H); 149.00 MHz (^{119}Sn)] spectrometers at ambient temperature. Solid state ^{119}Sn magic angle spinning (MAS) NMR measurements were carried out on a Bruker Avance II spectrometer at an external magnetic field of 9.4 T (i.e., 149.1 MHz, ^{119}Sn) using a standard Bruker 4 mm double-resonance H-X MAS probe. The samples were used "as synthesized", and spectra were recorded at a MAS spinning speed of 10 kHz. The isotropic chemical shifts were confirmed by measurements at variable spinning speeds. Transients (5000) were recorded for each measurement with a relaxation delay of 100 s. The spectra were referenced externally to $SnMe_4$ in $CDCl_3$ using solid SnO_2 as a secondary reference.

Preparation of [Me$_3$SnOZnMe]$_4$ (1). Dimethylzinc (0.99 g, 9.4 mmol) was dissolved in THF (20 mL) and slowly added to a suspension of trimethyltin hydroxide (1.7 g, 9.4 mmol), in THF (30 mL) at 0 °C. The reaction mixture was allowed to warm to room temperature overnight. All volatiles were removed in vacuo. Recrystallization of the residue from toluene at −20 °C affords **1** as colorless crystals. Yield: 2.3 g (2.4 mmol, 93%); mp: 262 °C (decomposition); ^{1}H-NMR(C_6D_6): δ = −0.422 ppm (s, 4H, Zn−CH_3), 0.355 ppm (s, 12H, Sn−(CH_3)$_3$, $^2J_{HSn}$ = 27.56 Hz/28.80 Hz); ^{13}C{^{1}H}-NMR (C_6D_6): δ = −14.01 ppm (Zn−CH_3), −2.44 ppm (Sn−(CH_3)$_3$, $^1J_{CSn}$ = 186.18 Hz/194.86 Hz); ^{119}Sn{^{1}H}-NMR (C_6D_6): δ = 139.28 ppm (Sn(CH$_3$)$_3$); $C_{16}H_{48}O_4Sn_4Zn_4$ (1044.02 g/mol); MS (Cl with NH_3) m/z (%) 1044.8 [M]$^+$ (56), 1027.7 [M − CH_4] $^+$ (19), 816.0 [M − $(CH_3)_3$-SnOH]$^+$ (68), 344.9 [$(CH_3)_3SnOSn(CH_3)_3$]$^+$ (97), 181.9 [$(CH_3)_3$-SnOH]$^+$ (91); EA(%) calcd.: C, 18.46; H, 4.65; found: C, 18.41; H, 4.49.

Preparation of [Me$_3$SnOZnEt]$_4$ (2). Analogous to the synthesis of 1, a solution of diethylzinc (0.53 g, 4.43 mmol), in THF (10 mL) was cooled at 0 °C and slowly treated with trimethyltin hydroxide (0.8 g, 4.43 mmol) in THF (20 mL) to give **2** as a white solid. Recrystallization from toluene leads to colorless crystals. Yield: 1.14 g (1.02 mmol, 95%); mp: 249 °C (decomposition); ^{1}H NMR (C_6D_6): δ = 0.29 ppm (m, 10H, 0.39 ZnCH$_2$CH_3, Sn(CH_3)$_3$, $^2J_{HSn}$ = 26.88 Hz/27.96 Hz), 1.52 ppm (t, ZnCH_2); ^{13}C{^{1}H}-NMR (C_6D_6): δ = −2.00 ppm (SnCH$_3$, $^1J_{CSn}$ = 185.87 Hz/194.62 Hz), −0.10 ppm(ZnCH$_2$CH$_3$), 14.02 ppm (ZnCH$_2$-CH_3). ^{119}Sn{^{1}H}-NMR (C_6D_6): δ = 137.13 ppm (−Sn(CH$_3$)$_3$); MS (EI): m/z (%) 1079.0 [M − C_2H_4] (79), 1068.9 [M − C_2H_6] (100), 957 [M − $(CH_3)_3$SnOH]$^+$ (40), 724.7 [M − $(CH_3)_3$SnOSn$(CH_3)_3$]$^+$ (33), 344.9 [$(CH_3)_3$SnOSn$(CH_3)_3$]$^+$ (52) 181.9 [$(CH_3)_3$SnOH]$^+$ (81); $C_{20}H_{56}O_4Sn_4Zn_4$ (1096.07 g/mol); EA (%): calcd.: C, 21.90; H, 5.15; found: C, 22.40; H, 4.91.

Single-Crystal X-ray Structure Determinations. Crystals were mounted on a glass capillary in perfluorinated oil and measured in a cold stream of N_2. The data for **1** and **2** were collected with a Oxford Diffraction Xcalibur S Saphire diffractometer at 150 K using Mo Kα radiation, λ = 0.7103 Å, ω-Scan). The structures were solved by direct methods. Refinement was carried out with the SHELX-97 software package.

Crystal Data for **1**. $C_{16}H_{48}O_4Sn_4Zn_4$, M = 1044 g/mol; monoclinic, space group $P2_1$; a = 11.2398(2) Å, b = 11.0673(2) Å, c = 16.6253(4) Å; β = 98.927(2)°; V = 2043.04(7) Å^3; D_c = 1.842 Mg/m^3; T = 150 K, 5139 reflections with [$I > 2\sigma(I)$], θ_{max} = 25.02°, R_1 = 0.0231, wR_2 = 0.0405 (all data).

Crystal Data for **2**. $C_{20}H_{56}O_4Sn_4Zn_4$, M = 1096 g/mol; monoclinic, space group $P2_1$; a = 11.3691(8) Å, b = 11.2041(6) Å, c = 17.6065(11) Å; β = 101.148(7)°; V = 2200.4(2) Å3; D_c = 1.795 Mg/m^3; T = 150 K, 7005 reflections with [$I > 2\sigma(I)$], θ_{max} = 25.05°; R_1 = 0.0776, wR_2 = 0.1639 (all data).

Full crystallographic data (CIF) can be obtained free of charge from the Cambridge Crystallographic Data Center [compound **1** CCDC (788764) compound **2** CCDC (788765)] at http://www.ccdc.cam.ac.uk/products/csd/request/.

Nanoparticle Preparation. Nanocrystalline materials with different composition, structure, and properties were prepared by thermolysis of SSPs **1** and **2** in a quartz tube oven. The degradation was carried out in synthetic dry air (20% O_2, 80% N_2) with variable heating times (2−36 h) and heating rates (5−30 K/min) to the final temperature (150, 350, 600 °C).

TFT Preparation. Si substrates for FET devices consisted of n-doped silicon coated with a 240 nm SiO_2 layer on which gold electrodes were deposited with an intermediate adhesive layer of indium tin oxide. The FET substrates were cleaned by sonication with 2-propanol, acetone, and water. The Sn-doped ZnO films were brought up by spin coating (30 s/1200 rpm) of the precursor mixture and calcination as described above.

Analytical Methods of the Degradation Products. Thermogravimetric analysis (TGA) of the precursors was carried out with a thermogravimetric setup from Rubotherm under dry synthetic air (20% O_2, 80% N_2) with a heating rate of 5 K/min, heating to 600 °C. TGA-FTIR measurements were performed with a TG STA 409 from Netsch and an Equinox 55 (Bruker) FTIR. The specific BET surface areas were measured using nitrogen adsorption at 78 K with a micromeritics Quantochrome Nova 4200e. Scanning electron microscopy (SEM) images were acquired using a Hitachi S-4000 microscope equipped with a SAMX EDX detector. The SEM samples were prepared by evaporating carbon on the samples. Transmission electron microscopy (TEM) images were recorded on a Tecnai G^2 20 S-TWIN (operating at 10 keV) located at the ZELMI, TU Berlin (Berlin Institute of Technology). The FTIR spectra were recorded from KBr pellets with a Perkin-Elmer 1000 series as ATR (attenuated total reflectance). Elemental analyses were performed on a Thermo Finnigan Flash EA 1112 Series. X-ray powder diffractograms were performed on a Bruker AXS D8 Advance instrument using Cu Kα radiation (λ = 1.5418 Å) and a position sensitive detector (PSD) in the 2θ range from 25 to 85° with a 0.015° step. The electrical resistivities were measured using the four-point probe method at room temperature, for which the instrument was assembled using a Keithley nanovoltmeter and a Keithley 2400 constant current source (Evonik, Marl). Melting points were recorded on a BSGT instrument, in sealed glass capillaries under nitrogen; the chemical composition was determined after thermal degradation in an autoclave (Berghof Labortechnik DAH) with an ICP-OES spectrometer [inductively coupled plasma optical emission spectrometry; Jobin Yvon 39+ in the laboratory of Prof. Schubert, TU-Berlin]. For the electrical characterization of the fabricated FET devices, a HP 4155A semiconductor parameter analyzer was employed.

ASSOCIATED CONTENT

Supporting Information. Additional spectroscopic data for compounds **1** and **2**, details on the single-crystal XRD characterization of precursors **1** and **2**, TGA-DTG of **2**, and TGA-IR of **1** as well as the characterization of the degradation products such as PXRD (for **1** under different conditions), EDX, IR, and FET characteristics for **1** (PDF, CIF). This material is available free of charge via the Internet at http://pubs.acs.org.

AUTHOR INFORMATION

Corresponding Author

*Phone: +49 (0)30-314-22265. Fax: +49 (0)30-314-29732. E-mail: matthias.driess@mailbox.tu-berlin.de.

■ ACKNOWLEDGMENT

We thank the Evonik Industries-Degussa (Marl) Science-to-Business Center Nanotronics (Marl) for fruitful cooperation and the Deutsche Forschungsgemeinschaft for financial support. We would also like to thank the ZELMI-team (Zentrales Laboratorium für Elektronenmikroskopie, TU-Berlin), the research group of Prof. Dr. Helmut Schubert, in particular Dr. Oliver Goerke (TU-Berlin) for ICP-OES and TGA-IR measurements, Manfred Dettlaff and Dr. Jan Dirk Epping for the NMR measurements, Dr. Vladimir Sepelak for sharing with us the chemical shift of Zn_2SnO_4 ($^{119}Sn\{^1H\}$ MAS NMR), and Dr. Matthew Asay and Dr. Carsten Präsang for helpful discussions.

■ REFERENCES

(1) (a) Veith, M. *J. Chem. Soc., Dalton Trans.* **2002**, 2405. (b) Barrelet, C. J.; Wu, Y.; Bell, D. C.; Lieber, C. M. *J. Am. Chem. Soc.* **2003**, *125*, 11498. (c) Veith, M.; Haas, M.; Huch, V. *Chem. Mater.* **2005**, *17*, 95. (d) Arndt, S.; Aksu, Y.; Driess, M.; Schomäcker, R. *Catal. Lett.* **2009**, *131*, 258. (e) Jana, S.; Aksu, Y.; Driess, M. *J. Chem. Soc., Dalton Trans.* **2009**, 1516. (f) Polarz, S.; Orlov, A.; Hoffmann, A.; Wagner, M. R; Rauch, C.; Kirste, R.; Gehlhoff, W.; Aksu, Y.; Driess, M.; van den Berg, M. W. E.; Lehmann, M. *Chem. Mater.* **2009**, *21*, 3889. (g) Heitz, S.; Aksu, Y.; Merschjann, C.; Driess, M. *Chem. Mater.* **2010**, *22*, 1376. (h) Heitz, S.; Epping, J.-D.; Aksu, Y.; Driess, M. *Chem. Mater.* **2010**, *22*, 4563. (i) Aksu, Y; Driess, M. *Angew. Chem., Int. Ed.* **2009**, *48*, 7778. (j) Ma, J.-G.; Aksu, Y.; Gregoriades, L. J.; Sauer, J.; Driess, M. *J. Chem. Soc., Dalton Trans.* **2010**, *39*, 103. (k) Rao, C. N. R. *Rev. Phys. Chem.* **1989**, *40*, 291. (l) Alivisatos, A. P. *Science* **1996**, *271*, 933. (m) Polarz, S.; Roy, A.; Merz, M.; Driess, M. *Small* **2005**, *1* (5), 540. (n) Heitz, S.; Aksu, Y.; Merschjann, C.; Driess, M.; *Chem. Eur. J.* **2011**, *17*, 3904. (o) Aksu, Y.; Frasca, S.; Wollenberger, U.; Driess, M.; Thomas, A. *Chem. Mat.* **2011**, DOI: 10.1021/cm103087p, in press.

(2) Look, D. C.; Claftin, B. *Phys. Status Solidi B* **2004**, *241*, 624.

(3) Meyer, K.; Alves, H.; Hofmann, D. M.; Kriegseks, W.; Forster, D.; Bertram, F.; Christen, J.; Hoffmann, A.; Strassburg, M.; Dworzak, M.; Haboeck, U.; Rodina, A. V. *Phys. Status Solidi B* **2004**, *241*, 231.

(4) Look, D. C.; Reynolds, C.; Litton, C. W.; Jones, R. L.; Eason, D. B.; Cantwell, G. *Appl. Phys. Lett.* **2002**, *81*, 1830.

(5) (a) Martinez, M. A.; Herrero, J.; Gutlerrez, M. T. *Sol. Energy Mater. Sol. Cells* **1997**, *45*, 75. (b) Anderson, N. A.; Ai, X.; Lian, T. Q. *J. Phys. Chem. B* **2003**, *107*, 14414. (c) Kreis, K.; Lindgren, J.; Lindquist, S. E.; Hagerfeldt, A. *Langmuir* **2000**, *16*, 4688.

(6) Huang, M. H.; Mao, S.; Feick, H; Yan, H. Q.; Wu., Y. Y.; Kind, H.; Weber, E.; Russo, R; Yang, P. D. *Science* **2001**, *292*, 1897.

(7) Lin, H. M.; Hsiau, P. J.; Tsai, W. L. *Nanostruct. Mater.* **1998**, *10*, 465.

(8) Willmer, H.; Kurtz, M.; Klementiev, K. V.; Tkachenko, O. P.; Grünert, W.; Hinrichsen, O.; Birkner, A.; Rabe, S.; Merz, K.; Driess, M; Wöll, C.; Muhler, M. *Phys. Chem. Chem. Phys.* **2003**, *5*, 4736.

(9) (a) Merz, K.; Block, S.; Schoenen, R.; Driess, M. *Dalton Trans.* **2003**, 3365.

(10) (a) Ilica Chang, C.-H. *Adv. Mater.* **2007**, *19*, 843. (b) Wang, R.; Sleight, A. W.; Cleary, D. *Chem. Mater.* **1996**, *8*, 433.

(11) (a) Caglar, M.; Caglar, Y.; Ilican, S. *Phys. Status Solidi C* **2007**, *3*, 1337. (b) Xu, L.; Su, Y.; Chen, Y.; Xiao, H.; Zhu, L.; Zhou, Q.; Li, S. *J. Phys. Chem. B* **2006**, *110*, 6637. (c) Krunks, M.; Mellikov, E. *Thin Solid Films* **1995**, *270*, 33. (d) Jeong, S.; Ha, Y.-G.; Moon, J.; Facchetti, A.; Marks, T. J. *Adv. Mater.* **2009**, *21*, 1. (e) Mensinger, Z. L.; Gatlin, J. T.; Meyers, S. T.; Zakharov, L. N.; Keszler, D. A.; Johnson, D. W. *Angew. Chem., Int. Ed.* **2008**, *47*, 9484. (f) Ong, B. S.; Li, C.; Li, Y.; Wu, Y.; Loutfy, R. *J. Am. Chem. Soc.* **2007**, *129*, 2750. (g) Lee, D.-H.; Chang, Y.-J.; Herman, G. S.; Chang, C.-H. *Adv. Mater.* **2007**, *19*, 843. (h) Kapoor, P. N.; Heroux, D.; Mulukulta, R. S.; Zaikovski, V.; Klabunde, K. J. *J. Mater. Chem.* **2003**, *13*, 410. (i) Seisenbaera, G. A.; Suslova, E. V; Kritikos, M.; Kessler, V. G.; Rapenne, L.; Andrieux, M.; Chassagneux, F.; Parola, S. *J. Mater. Chem.* **2004**, *14*, 3150. (j) Kessler, V. G.; Gohil, S.; Parola, S. *Dalton Trans.* **2003**, 544. (k) Orlov, A.; Roy, A.; Lehmann, M.; Driess, M.; Polarz, S. *J. Am. Chem. Soc.* **2007**, *129*, 371.

(12) Nomura, K.; Ohta, H.; Ueda, K.; Kamiya, T.; Hirano, M.; Hosono, H. *Science* **2003**, *300*, 1269.

(13) Ogo, Y.; Nomura, K.; Yanagi, H.; Kamiya, T.; Hirano, M.; Hosono, H. *Phys. Status Solidi A* **2008**, *205*, 1920.

(14) (a) Kim, M.-G.; Kim, H. S.; Ha, Y. G.; Kanatzidis, M. G.; Facchetti, A.; Marks, T. J. *J. Am. Chem. Soc.* **2010**, *132*, 10352. (b) Couttus, T. J.; Young, D. L.; Li, X; Mulligan, W. P.; Wu, X. *J. Vac. Sci. Technol., A* **2000**, *18*, 2646.

(15) Sun, M.; Zhang, Q. F.; Wu, J. L. *J. Phys. D: Appl. Phys.* **2007**, *40*, 3798.

(16) Deng, R.; Zhang, X. T. *J. Phys. Chem. C* **2007**, *111*, 13013.

(17) Ortega, Y.; Fernandez, P.; Piqueras, J. *Nanotechnology* **2007**, *18*, 115606.

(18) Li, S. Y.; Lin, P.; Lee, C. Y T.; Tseng, Y.; Huang, C. J. *J. Phys: Appl. Phys.* **2004**, *37*, 2274.

(19) Bae, S. Y.; Na, C. W.; Kang, J. H.; Park, J. *J. Phys. Chem. B* **2005**, *109*, 2526.

(20) Fang, X. S.; Ye, C. H.; Zhang, L. D.; Li, Y.; Xiao, Z. D. *Chem. Lett.* **2005**, *34*, 436.

(21) Chen, H. S.; Qi, J. J.; Huang, Y. H.; Liao, Q. L.; Zhang, Y. *Acta Phys. Chim.* **2007**, *23*, 155.

(22) Roy, A.; Polarz, S.; Rabe, S. M.; Rellinghausen, B.; Zahres, H.; Kruis, F. E.; Driess, M. *Chem.—Eur. J.* **2004**, *10*, 1565.

(23) (a) Cho, S.; Ma, J.; Kim, Y.; Sun, Y.; Wong, G. K. L; Ketterson, J. B. *Appl. Phys. Lett.* **1999**, *75*, 2761. (b) Rozgonyi, G. A.; Polito, W. J. *Appl. Phys. Lett.* **1966**, *8*, 220. (c) Kaneko, D.; Shouji, H. *Langmuir* **2000**, *16*, 4086.

(24) (a) Bahnemann, D. W.; Kormann, C.; Hoffmann, M. R. *J. Phys. Chem.* **1987**, *91*, 3789. (b) Spanhel, L.; Andersen, M. A. *J. Am. Chem. Soc.* **1991**, *113*, 2826.

(25) Driess, M.; Merz, K.; Rell, S. *Eur. J. Inorg. Chem.* **2000**, 2517.

(26) Domingos, A. M.; Sheldrick, G. M. *Acta Crystallogr.* **1974**, *B30*, 519.

(27) Polarz, S.; Roy, A.; Merz, M.; Halm, S.; Schröder, D.; Schneider, L.; Bacher, G.; Kruis, F. E.; Driess, M. *Small* **2005**, *5*, 540.

(28) Schumann, H.; Schumann, I.; Gmelin *Handbook of Inorganic and Organometallic Chemistry*, 8th ed.; Organotin Compounds, Springer: Berlin, 1984; Vol. 11, pp 50−56.

(29) Merz, K.; Hu, H.; Rell, S.; Driess, M. *Eur. J. Inorg. Chem.* **2003**, 51.

(30) Merz, K.; Block, S.; Schoenen, R.; Driess, M. *Dalton Trans.* **2003**, 3365.

(31) Bond, A. D.; Linton, D. J.; Whetley, E. H. *Acta Crystallogr.* **2001**, *E57*, 298.

(32) Jana, S.; Berger, R. J. F.; Fröhlich, R.; Pape, T.; Mitzel, N. W. *Inorg. Chem.* **2007**, *46*, 4293.

(33) (a) Merz, K.; Schoenen, R.; Driess, M. *J. Phys. IV France* **2001**, *11*, Pr3–467. (b) Schoenen, R.; Merz, K.; Rell, S.; Driess, M. *J. Phys. IV France* **2001**, *11*, Pr3–547. (c) Polarz, S.; Roy, A.; Merz, M.; Halm, S.; Schröder, S.; Schneider, L.; Bacher, G.; Driess, M. *Small* **2005**, *1*, 540. (d) Trindade, T.; OBrien, P; Pickett., N. L. *Chem. Mater.* **2001**, *13*, 3443 .

(34) MacKenzie, K. J. D.; Smith, M. E.; Pergamon Materials Series. *Multinuclear Solid-State NMR of Inorganic Materials,* 2002, 6; Elsiever Science Ltd: Oxford, U.K.

(35) Sepelak, V.; Becker, K. D. *Chem. Mater.* **2009**, *21*, 2518.

(36) Sepelak, V. Institute of Nanotechnology, Karlsruhe Institute of Technology, unpublished work, 2010.

(37) (a) Ong, B. S.; Li, C.; Li, Y.; Wu, Y.; Loutfy, R. *J. Am. Chem. Soc.* **2007**, *129*, 2750. (b) Cheng, H.; Chen, C.; Tsay, C. Y. *Appl. Phys. Lett.* **2007**, *90*, 012113. (c) Lee, D. H.; Chang, Y. J.; Hermann, G. S; Chang, C. H. *Adv. Mater.* **2007**, *19*, 843.

(38) (a) Pang, C.; Yan, B.; Liao, L.; Liu, B.; Zheng, Z.; Wu, T.; Sun, H.; Yu, T. *Nanotechnology* **2010**, *21*, 465706. (b) Alpuche-Aviles, M. A.; Wu, Y. *J. Am. Chem. Soc.* **2009**, *131*, 3216.

(39) (a) Jeong, S.; Yeongi, J.; Moon, J. *J. Phys. Chem. C* **2008**, 11082. (b) Ali, H. M. *Phys. Status Solidi A* **2005**, *202*, 2742.

(40) (a) Sheng, S. Y.; Thia-Shu, Z. *Sens. Actuators, B* **1993**, *12*, 5. (b) Kovecera, D.; Petrov, K. *Solid State Ionics* **1998**, *109*, 327.
(41) Wang, C.; Wang, X.; Mai, J. C.; Sheng, G. Y.; Peng, P.; Fu, M. *J. Mater. Sci.* **2002**, *37*, 2989. (b) Yu, J. H.; Choi, G. M. *Sens. Actuators* **2001**, *72*, 141.
(42) Rong, A.; Gao, X. P; Song, D. Y. *J. Phys. Chem. B* **2006**, *110*, 14754.
(43) Tan, B.; Toman, E.; Li, Y.; Wu, Y. *J. Am. Chem. Soc.* **2007**, *129*, 4162.
(44) Stambolova, I. *J. Solid State Chem.* **1997**, *128*, 305.
(45) Nikolic, N.; Sreckovic, T.; Ristic, M. M. *J. Eur. Ceram. Soc.* **2001**, *21*, 2071.
(46) Couttus, T. J.; Young, D. L.; Li, X; Mulligan, W. P.; Wu, X. *J. Vac. Sci. Technol., A* **2000**, *18*, 2646.
(47) Polarz, S.; Orlov, A.; Schüth, F.; Lu, A. H. *Chem.—Eur. J.* **2007**, *13*, 592.
(48) Wang, L.; Zhang, X.; Liao, X. *Nanotechnology* **2005**, *16*, 2928.